SCIENCE CHINA Materials

Design and synthesis of low band gap non-fullerene acceptors for organic solar cells with impressively high J_{sc} over 21 mA cm^{-2}

Gao Huan-Huan, Sun Yanna, Wan Xiangjian, Kan Bin, Ke Xin, Zhang Hongtao, Li Chenxi and Chen Yongsheng

Citation: SCIENCE CHINA Materials **60**, 819 (2017); doi: 10.1007/s40843-017-9084-x

View online: http://engine.scichina.com/doi/10.1007/s40843-017-9084-x

View Table of Contents:http://engine.scichina.com/publisher/scp/journal/SCMs/60/9

Published by the Science China Press

SCIENCE CHINA Materials

ARTICLES

mater.scichina.com link.springer.com

Published online 29 August 2017 | doi: 10.1007/s40843-017-9084-x
Sci China Mater 2017, 60(9): 819–828

Design and synthesis of low band gap non-fullerene acceptors for organic solar cells with impressively high J_{sc} over 21 mA cm^{-2}

Huan-Huan Gao, Yanna Sun, Xiangjian Wan*, Bin Kan, Xin Ke, Hongtao Zhang, Chenxi Li and Yongsheng Chen*

ABSTRACT **Three low bandgap non-fullerene acceptors based on thieno[3,2-b]thiophene fused core with different ending groups, named TTIC-M, TTIC, TTIC-F were designed and synthesized. Using a wide bandgap polymer PBDB-T as donor to form a complementary absorption in the range of 300–900 nm, high efficencies of 9.97%, 10.87% and 9.51% were achieved for TTIC-M, TTIC and TTFC-F based photovoltaic devices with impressively high short circuit current over 21 mA cm^{-2}.**

Keywords: A-D-A type, non-fullerene acceptors, low bandgap, high short circuit current values

INTRODUCTION

Fullerene derivatives as the acceptor materials have been widely used in organic solar cells (OSCs) [1–5] and power conversion efficiencies (PCEs) over 10% have been achieved thanks to the new donor materials design and device optimizations [6–8]. Recently, non-fullerene acceptors (NFAs) have challenged the fullerene derivatives dominated positions owing to the easily tuned energy levels, broadened absorptions and facile synthesis process [9–14]. It is worthy to note that PCEs over 12% have been realized for the non-fullerene based OSCs, which opens a very promising avenue [15,16].

Presently, the mostly successful non-fullerene acceptors are the small molecules with acceptor-donor-acceptor (A-D-A) structure, in which conjugated fused units are employed as the central building blocks and electron withdrawing groups, mostly 3-(dicyanomethylidene)-indan-1-one and its derivatives are used as the end units [10]. Their properties such as the energy levels and absorptions. could be tuned through the delicate chemical structure design [17,18]. For example, 4,9-dihydro-s-indaceno[1,2-b:5,6-b']-dithiophene (**IDT**)[19–21] and 6,12-dihydro-dithieno[2,3-d:2',3'-d']-s-indaceno[1,2-b:5,6-b'] dithiophene (**IDTT**)[10,18] were used as the central building blocks to construct the A-D-A NFAs such as **ITIC** [10], **ITIC-Th** [22] and **IT-M** [21,23], etc. with 3-(dicyanomethylidene)-indan-1-one and its derivatives as the end groups, and PCE over 11% have been achieved.

On the other hand, in order to achieve high photovoltaic performances, it is essential for the donor or acceptor materials to have complementary absorptions covering the visible light to the near-infrared region in order to get high short circuit current (J_{sc}) values. To this end, the strategy of using wide bangap donor materials and low bandgap acceptor materials to blend as the active layers has been proved to be an efficient way [21,24]. Recently, the low band gap NFAs such as **IEICO** [24], **IT-4F** [16], **INIC3** [25], etc. have been reported and gave high PCEs over 10% with J_{sc} over 19 mA cm^{-2}.

Recently, our group reported NFA **FDICTF** [26] and **NFBDT** [27] by fusing fluorene or BDT units with adjacent thiophenes. In contrast to the unfused counterparts, the two NFAs showed red shifted absorptions and balanced charge mobilities after blending with the donor materials and PCE over 10% was achieved.

Thieno[3,2-b]thiphene (TT) has been widely used in OSC partially due to a stable quinoid structure, the strong electron-donating ability and the coplanar structure [28,29]. Herein we utilized the thieno[3,2-b]thiphene as the central building block fused with another two thiophene units by the sp^3 carbon linked with four 4-hexylbenzene groups to improve the solubility and inhibit the molecular excessive aggregation [30–32]. With the above

State Key Laboratory of Elemento-Organic Chemistry, Centre of Nanoscale Science and Technology and Key Laboratory of Functional Polymer Materials, College of Chemistry, Nankai University, Tianjin 300071, China
* Corresponding authors (emails: xjwan@nankai.edu.cn (Wan X); yschen99@nankai.edu.cn (Chen Y))

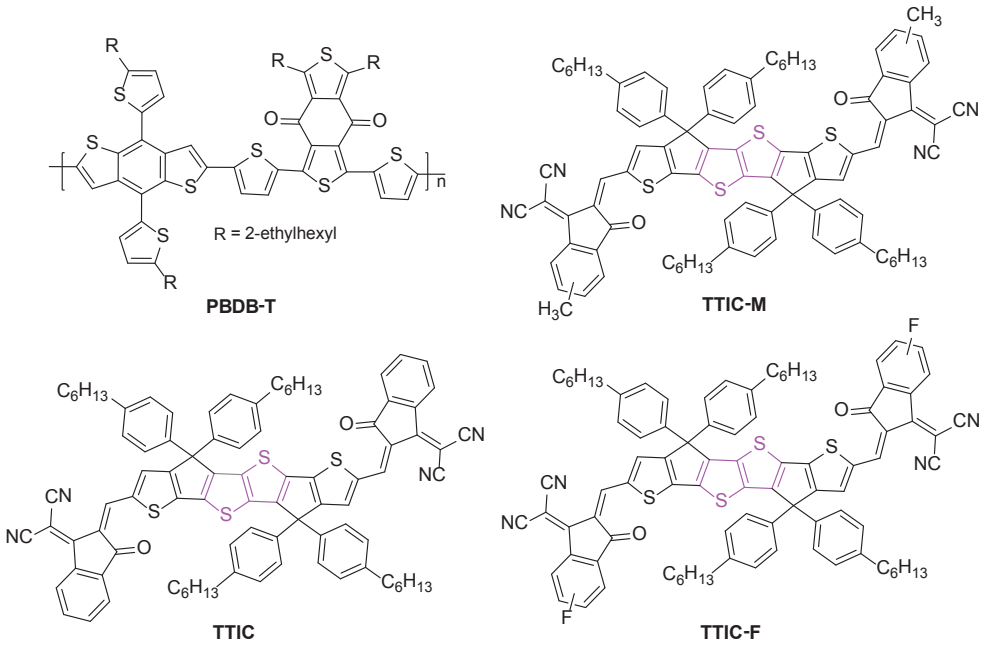

Figure 1 Chemical structure of **PBDB-T** and three non-fullerene acceptors.

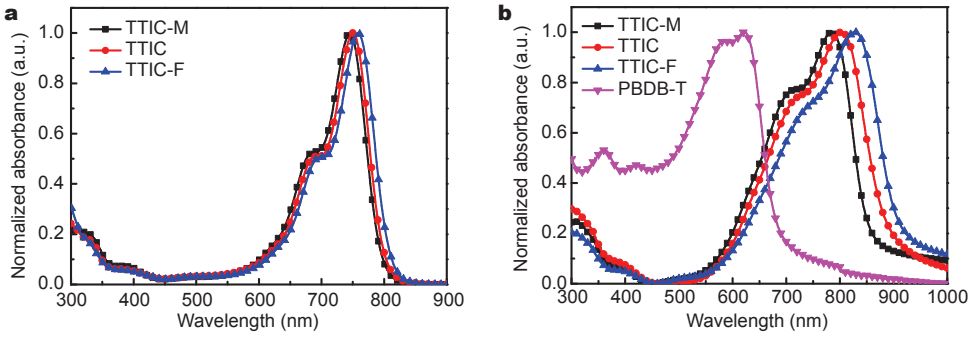

Figure 2 UV-vis spectra of **TTIC-M**, **TTIC** and **TTIC-F** in the dilute chloroform solution (a) and thin films.

thieno[3,2-b]thiphene and thiophene fused unit as the core, three NAFs named **TTIC-M**, **TTIC**, **TTIC-F** were prepared with 3-(dicyanomethylidene)-indan-1-one and its two derivatives substituted with methyl or fluorine as the end groups (Fig. 1). The purpose of introducing the methyl and fluorine substituted indanone groups with electron pushing and pulling abilities is to subtly tune the energy levels and absorptions and investigate the effects on photovoltaic performances. As expected, **TTIC-M**, **TTIC** and **TTIC-F** exhibit near-infrared absorptions with maximum absorption (λ_{max}) of 783, 820 and 828 nm in the thin films (Fig. 2) and low optical bandgaps of 1.44, 1.38 and 1.35 eV, respectively. For device fabrication, a widely used wide bandgap polymer donor poly[(2,6-(4,8-bis(5-(2-ethylhexyl)thiophen-2-yl)benzo[1,2b:4,5b']dithiophene)-*alt*-(5,5-(1',3'-di-2-thienyl-5',7')-bis(2-ethylhexyl)-benzo[1',2'-c:4',5'-c']dithiophene-4,8-dione)] (**PBDB-T**) [33] was selected as the donor material. The optimized PCEs of 9.97%, 10.87% and 9.51% were obtained for **TTIC-M**, **TTIC** and **TTIC-F** based devices with impressively high J_{sc} of 19.07, 20.58 and 21.26 mA cm^{-2}, respectively. It is worthy to note that Wang *et al.* [34] reported the molecule **TTIC** with the PCE of 9.77% with **PTB7-Th** as donor material when we were preparing this manuscript.

The detailed synthesized routes are shown in Scheme 1 and the corresponding characterization data are shown in the Supplemenary information (SI). The related ^{1}H NMR, ^{13}C NMR spectrum and HR-MS mass spectrometry also attached in the SI. All of the **TTIC-M**, **TTIC** and **TTIC-F**

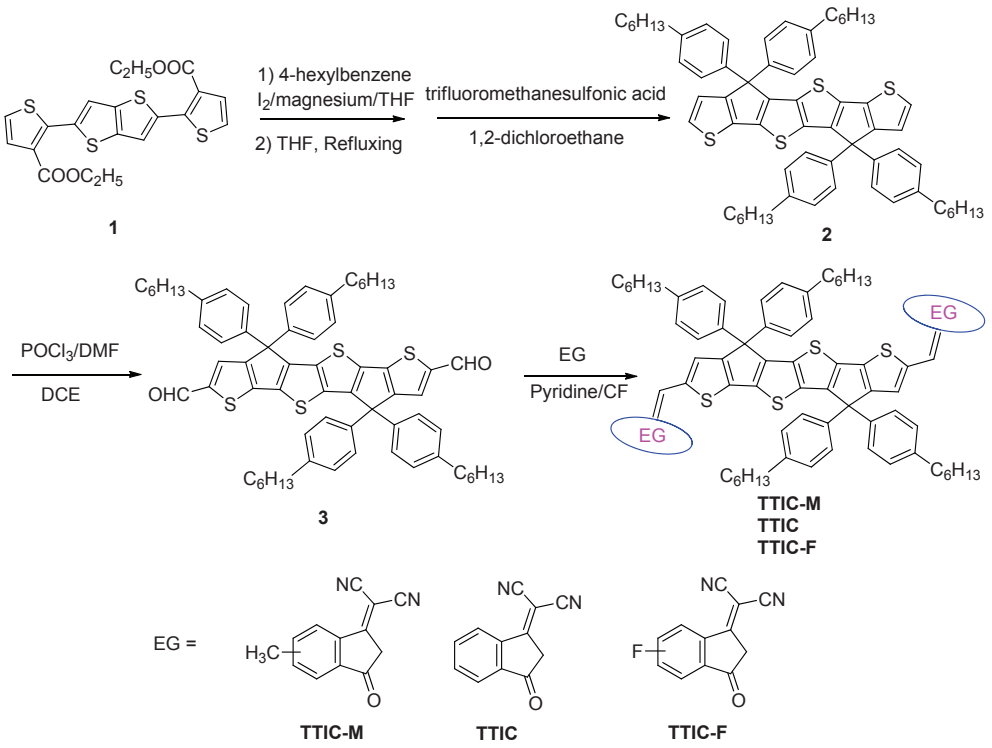

Scheme 1 The synthetic routes of **TTIC-M**, **TTIC** and **TTIC-F**.

exhibit preferable thermal stability up to 370, 350 and 350°C under nitrogen atmosphere by thermogravimetric analysis (TGA) (Fig. S1).

EXPERIMENTAL SECTION

Materials

All reagents and solvents were purchased from commercial corporation and used without further purification. All the reactions and manipulations were carried out under the protection of argon. The polymer donor **PBDB-T** was purchased from 1-Material Inc.

Synthesis

The intermediate **1** was synthesized according to the reported literature [35]. Compound **1** was processed with hexylbenzene Grignard reagent and then reacted with trifluoromethanesulfonic acid as the catalyst to achieve the cyclization intermediate **2**. Compound **3** was obtained from synthon **2** *via* Vilsmeier-Haack reaction. Then the target acceptor materials were synthesized from the precursor **3** with subsequent Knovenagel condensation.

Synthesis compound 2

Under argon, hexylbenzene (1.613 g, 6.690 mmol), a small quantity of iodine, and magnesium chips (267 mg, 11.13 mmol) were dissolved in anhydrous tetrahydrofuran (THF) (10 mL). The reaction was triggered by blower and stirred at room temperature for ten minutes. Then the 4-*n*-hexylphenyl magnesium bromide synthesized above was added into the reaction system of **1** (500 mg, 1.115 mmol) in anhydrous THF (20 mL) dropwise under argon. The reaction was refluxed for another 12 h. The reaction solution was washed with brine for three times and dried over anhydrous Na_2SO_4. The solvent was removed under vacuum. The crude product was dissolved in 1,2-dichloroethane (30 mL) and three drops of trifluoromethanesulfonic acid was added as the catalyst. The reaction solution was stirred at 65°C for 30 min and quenched with 10 mL ice water and washed with water for four times. The solvent was removed under vacuum, and the crude product was purified by column chromatography using CH_2Cl_2/PE (1:40) as the eluent to give compound **2** as a yellow solid (60%). ^{1}H NMR (400 MHz, $CDCl_3$) δ 7.17–7.13 (m, 10H), 7.08–7.05 (m, 10H), 2.54 (t, 8H), 1.59–1.53 (m, 8H), 1.30–1.25 (m, 24H), 0.88–0.84 (m, 12H). ^{13}C NMR (101 MHz, $CDCl_3$) δ 157.00, 148.41, 141.75, 139.87, 137.11, 136.85, 134.91, 128.50, 127.80, 125.26, 123.27, 61.91, 35.61, 31.73, 31.30, 29.17, 22.61, 14.12. HR-MS (MALDI): *m*/*z* $[M]^+$ calcd. for $C_{64}H_{72}S_4$,

968.4517; found, 968.4518.

Synthesis of compound 3

Under argon, anhydrous *N*,*N*-dimethylformamide (3 mL) was added. Then anhydrous phosphorus oxychloride ($POCl_3$) (200 μL) was injected into the reaction system dropwise in the ice-water bath. The reaction mixture was stirred under 0°C for another 30 min, and then stirred at room temperature for 3 h to gain the Vilsmerier reagent. A solution of **2** in 1,2-dichloroethane (DCE, 80 mL) was degassed with argon for 15 min and then the Vilsmerier reagent was added into the reaction slowly and stirred at room temperature for 1 h. The reaction solution was stirred at 85°C for another 12 h. 20 mL saturated sodium acetate solution was added slowly to quench the reaction. The reaction solution was washed with water for three times and dried over anhydrous Na_2SO_4. The solvent was removed under vacuum, and the crude product was purified by column chromatography using CH_2Cl_2/PE (1:1) as the eluent to give compound **3** as a yellow solid (90%). ^{1}H NMR (400 MHz, $CDCl_3$) δ 9.80 (s, 2H), 7.68 (s, 2H), 7.12 (s, 16H), 2.58–2.54 (m, 8H), 1.60–1.55 (m, 12H), 1.30–1.26 (m, 20H), 0.86 (t, J = 6.8 Hz, 12H). ^{13}C NMR (101 MHz, $CDCl_3$) δ 182.47, 157.98, 152.37, 146.96, 144.26, 142.62, 138.27, 138.15, 137.63, 131.65, 128.88, 127.56, 62.30, 35.58, 31.69, 31.26, 29.10, 22.59, 14.09. HR-MS (MALDI): m/z $[M]^+$ calcd. for $C_{66}H_{72}O_2S_4$, 1024.4415; found, 1024.4403.

*Synthesis of **TTIC***

A mixture of compound **3** (100 mg, 0.0975 mmol), 3-(dicyanomethylidene)-indan-1-one (56 mg, 0.288 mmol) in chloroform 30 mL under argon was stirred at room temperature for 12 h. The organic phase was washed with water for three times and dried over anhydrous Na_2SO_4. The solvent was removed under vacuum, and the crude product was purified by column chromatography using CF/PE (1:1) as the eluent to give compound **TTIC** as a green solid (85%). ^{1}H NMR (400 MHz, $CDCl_3$) δ 8.86 (s, 2H), 8.68 (dd, J = 6.3, 1.5 Hz, 2H), 7.92–7.88 (m, 2H), 7.78–7.72 (m, 4H), 7.71–7.69 (m, 2H), 7.14 (s, 16H), 2.58 (t, 8H), 1.63–1.55 (m, 12H), 1.32–1.27 (m, 20H), 0.89–0.84 (m, 12H). ^{13}C NMR (101 MHz, $CDCl_3$) δ 188.50, 160.33, 159.52, 155.48, 154.52, 151.27, 142.91, 140.52, 140.14, 140.00, 139.74, 139.61, 138.69, 137.94, 137.79, 136.82, 135.01, 134.29, 129.04, 127.58, 125.24, 123.65, 121.39, 114.88, 114.84, 77.33, 77.01, 76.69, 62.25, 35.59, 31.68, 31.23, 29.09, 22.58, 14.08. HR-MS (MALDI): m/z $[M]^+$ calcd. for $C_{90}H_{80}N_4O_2S_4$, 1376.5164; found, 1376.5165.

*Synthesis of **TTIC-M***

The synthetic procedure was the same as **TTIC**. And the crude product was purified by column chromatography using CF/PE (1:1) as the eluent to give **TTIC-M** as a green solid (80%). ^{1}H NMR (400 MHz, $CDCl_3$) δ 8.83 (s, 2H), 8.54 (d, J = 8.1 Hz, 1H), 8.46 (s, 1H), 7.79 (d, J = 7.7 Hz, 1H), 7.68 (s, 3H), 7.53 (t, J = 7.0 Hz, 2H), 7.14 (s, 16H), 2.58 (t, 8H), 2.55–2.51 (m, 6H), 1.66–1.53 (m, 12H), 1.31–1.26 (m, 20H), 0.89–0.83 (m, 12H). ^{13}C NMR (101 MHz, $CDCl_3$) δ 188.27, 160.46, 159.36, 154.30, 146.59, 146.06, 142.86, 140.40, 140.04, 139.58, 138.46, 137.87, 137.64, 137.18, 135.88, 135.29, 134.69, 129.02, 127.59, 125.61, 125.19, 123.55, 121.94, 115.01, 114.95, 77.34, 77.23, 77.02, 76.70, 62.22, 35.60, 31.69, 31.25, 29.10, 22.59, 22.07, 14.10. HR-MS (MALDI): m/z $[M]^+$ calcd. for $C_{92}H_{84}N_4O_2S_4$, 1404.5477; found, 1404.5492.

*Synthesis of **TTIC-F***

The synthetic procedure was the same as **TTIC**. The crude product was purified by column chromatography using CF/PE (1:1) as the eluent to give **TTIC-F** as a green solid (90%). Since the effect of fluorine atom, we have not got the ^{13}C NMR spectrum. ^{1}H NMR (400 MHz, $CDCl_3$) δ 8.87 (s, 2H), 8.38 (d, J = 8.9 Hz, 2H), 7.96–7.87 (m, 2H), 7.76–7.71 (m, 2H), 7.46–7.39 (m, 2H), 7.16 (s, 16H), 2.61 (t, 8H), 1.64–1.58 (m, 12H), 1.31–1.28 (m, 20H), 0.91–0.86 (m, 12H). HR-MS (MALDI): m/z $[M]^+$ calcd. for $C_{90}H_{78}F_2N_4O_2S_4$, 1412.4976; found, 1412.5003.

Fabrication of OSCs

The indium tin oxide (ITO)-coated glass substrates were cleaned by ultrasonic treatment in detergent, deionized water, acetone, and isopropyl alcohol under ultrasonication for 15 min each and subsequently dried by nitrogen blow. A thin layer of PEDOT:PSS (Clevios P VP AI 4083, filtered at 0.45 μm) was spin-coated at 3000 rpm onto the ITO surface. After being baked at 150°C for 20 min, the substrates were transferred into an argon-filled glovebox. The donor material **PBDB-T** and the acceptor materials **TTIC-M**, **TTIC** and **TTIC-F** were dissolved in chlorobenzene to generate 20 mg mL^{-1} blend solutions with the donor/acceptor weight ratio of 1:1. In fabrication, the active layer was exposed to chloroform vapor for 90 s to optimize the morphology. A thin layer of PDINO and an 80 nm Al layer were deposited on the active layer under high vacuum (<2 × 10^{-4} Pa).

Characterization and measurements

The ^{1}H and ^{13}C nuclear magnetic resonance (NMR) spectra were taken on a Bruker AV400 Spectrometer. The

HR-MS data were recorded on Varian 7.0T FT-MS. The TGA was carried out on a NETZSCH STA 409PC instrument under purified nitrogen gas flow with a heating rate of 15°C min^{-1}, UV–vis spectra were obtained with a JASCO V-570 spectrophotometer. Photoluminescence (PL) spectra were measured with a FL-4600 fluorescence spectrometer (Hitachi, Japan) equipped with a plotter unit. Cyclic voltammetry (CV) experiments were performed with a LK98B II microcomputer-based Electrochemical Analyzer. All CV measurements were carried out at room temperature with a conventional three-electrode configuration employing a glassy carbon electrode as the working electrode, a saturated calomel electrode (SCE) as the reference electrode, and a Pt wire as the counter electrode. Dichloromethane was distilled from calcium hydride under dry nitrogen immediately prior to use. Tetrabutylammonium phosphorus hexafluoride (Bu_4NPF_6, 0.1 mol L^{-1}) in dichloromethane was used as the supporting electrolyte; the scan rate was 100 mV s^{-1}. Atomic force microscopy (AFM) was performed using a MultiMode 8 atomic force microscope in tapping mode. Space-charge-limited-current (SCLC) mobility was measured using a diode configuration of ITO/PEDOT:PSS/PBDB-T:acceptor/Au for hole and Al/PBDB-T:acceptor/Al for electron by taking the dark current density in the range of 0–2 V and fitting the results to a space charge limited form, where the SCLC is described by:

$$J=\frac{9\varepsilon_0\varepsilon_r\mu_0 V^2}{8L^3},$$

where J is the current density, L is the film thickness of the active layer, μ_0 is the hole or electron mobility, ε_r is the relative dielectric constant of the transport medium, ε_0 is the permittivity of free space (8.85×10^{-12} F m^{-1}), V (= $V_{appl} - V_{bi}$) is the internal voltage in the device, where V_{appl} is the applied voltage to the device and V_{bi} is the built-in voltage due to the relative work function difference of the two electrodes. The current density-voltage (J-V) curves of photovoltaic devices were obtained by a Keithley 2400 source-measure unit. The photocurrent was measured under illumination simulated 100 mW cm^{-2} AM 1.5G irradiation using a xenon-lamp-based solar simulator [SAN-EI XES-70S1 (AM 1.5G)] in an argon filled glovebox. External quantum efficiencies (EQE) were measured using Stanford Re-search Systems SR810 lock-in amplifier.

RESULTS

Photophysical and electrochemical properties

The UV-vis absorption spectra in dilute chloroform solution and thin films are shown in Fig. 2 and the corresponding photophysical data are summarized in Table 1. As shown in Fig. 2a, **TTIC-M**, **TTIC** and **TTIC-F** in their solution all show broad and red-shifted absorption around 600–800 nm, with the λ_{max} peaks located at 746, 750 and 756 nm and relatively weaker shoulder peaks at 680, 686 and 695 nm, respectively. As for the thin films, they display evidently broad and red-shifted absorption peaks at 783, 820 and 828 nm. The polymer donor shows complementary absorption ranging from 500−750 nm. The red-shifted absorption properties are mainly attributed to the strong electron-donating performances of central core and intense intramolecular charge transfer. In order to further understand the charge transfer properties between the donor and acceptor, the PL quenching effect was tested (Fig. 3) . It is worth noting that all the pure films based on **PBDB-T** and **TTIC** derivatives show clear PL spectra in the region of 650–800 nm and 800–900 nm, respectively. While the blend films exhibit strong PL quenching effect, indicating the efficient photoinduced charge transfer between the donor and acceptor materials. CV measurements were performed in dichloromethane solution and calibrated against ferrocene (4.4 eV below vacuum), the supporting electrolyte contains 0.1 mol L^{-1} tetrabutylammonium hexafluorophosphate ($TBAPF_6$), under a scan rate of 100 mV s^{-1} (Fig. 4). The highest occupied molecular orbital (HOMO) and lowest unoccupied molecular orbital (LUMO) energy levels of **TTIC-M**, **TTIC** and **TTIC-F** were obtained from the onset oxidation and reduction potential with values of −5.30, −5.33, −5.34 and −3.82, −3.87, −3.88 eV, respectively. The HOMO energy levels offset between the three acceptors and **PBDB-T** (−5.28 eV) are as low as 0.10 eV

Table 1 Summay of the photophysical and electronic data of **TTIC-M**, **TTIC** and **TTIC-F**

Compound	λ_{max}^{sol} (nm)	λ_{max}^{film} (nm)	λ_{edge}^{film} (nm)	E_g^{opt} (eV)	HOMO (eV)	LUMO (eV)	E_g^{cv} (eV)
TTIC-M	746	783	863	1.44	−5.30	−3.82	1.48
TTIC	750	820	900	1.38	−5.33	−3.87	1.46
TTIC-F	756	828	916	1.35	−5.34	−3.88	1.46

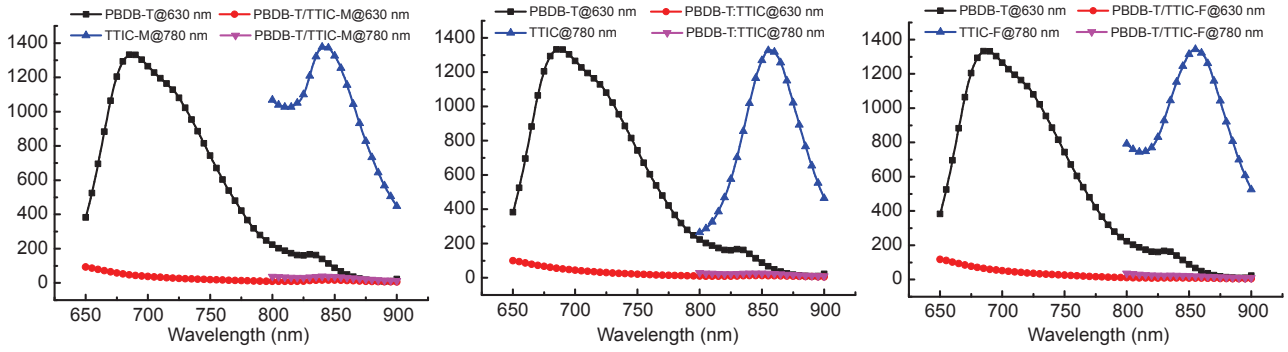

Figure 3 PL spectra of **PBDB-T**, **TTIC-M**, **TTIC**, **TTIC-F** and the blend films of **PBDB-T** and **TTIC** derivatives.

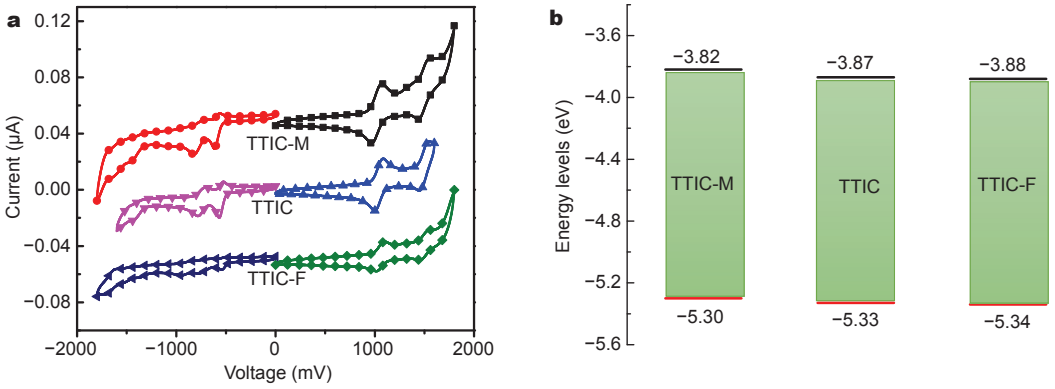

Figure 4 CVs of **TTIC-M**, **TTIC** and **TTIC-F** in dichloromethane (a) and the corresponding energy levels (b).

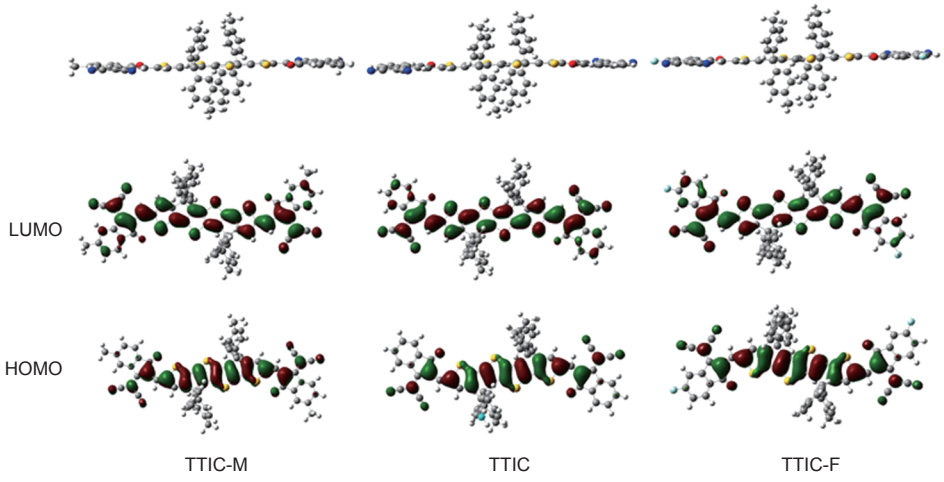

Figure 5 The geometry and the HOMOs, LUMOs distribution by DFT calculations.

(0.02, 0.05 and 0.06 eV, respectively), suggesting small ΔE_H is not the necessary restriction for the non-fullerene OSC as evidenced below.

DFT calculation

Density functional theory (DFT) calculations at the B3LYP/6-31G(d) level were performed to further investigate the electron distribution and geometry of the three acceptors. The hexyl groups were replaced by methyl to simplify computational process. Like other NFAs cases, the electron cloud densities of HOMO and LUMO are mainly localized at the central fused donor cores and

Table 2 Photovoltaic parameters of the BHJ solar cells based on **PBDB-T** and the three non-fullerene acceptors

Compound	V_{oc} (V)	$J_{sc}^{J\text{-}V}$ (mA cm^{-2})	J_{sc}^{EQE} (mA cm^{-2})	FF	PCE[c] (%)
TTIC-M	0.83[a]	18.36[a]		0.56[a]	8.39 ± 0.14 (8.53)[a]
	0.83[b]	19.07[b]	17.58	0.63[b]	9.85 ± 0.12 (9.97)[b]
TTIC	0.81[a]	18.78[a]		0.63[a]	9.41 ± 0.17 (9.58)[a]
	0.80[b]	20.58[b]	19.37	0.66[b]	10.73 ± 0.14 (10.87)[b]
TTIC-F	0.72[a]	19.11[a]		0.59[a]	7.92 ± 0.16 (8.08)[a]
	0.71[b]	21.26[b]	19.31	0.63[b]	9.38 ± 0.13 (9.51)[b]

a) The devices without post process. b) SVA for 90 s. c) The PCE values were measured from 30 devices and the highest PCE were in parentheses.

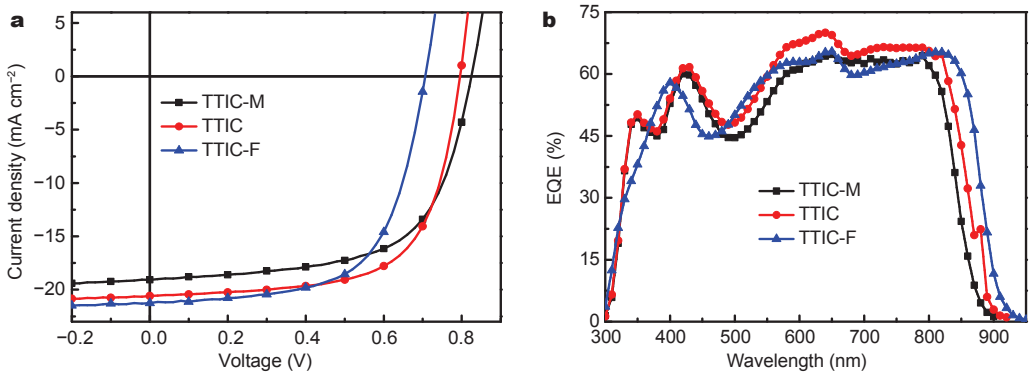

Figure 6 The *J-V* curves based on **PBDB-T**/**TTIC-M**, **TTIC** and **TTIC-F** with SVA for 90 s (a) and the corresponding EQE spectra (b).

the acceptor end groups, respectively (Fig. 5).

OSCs performances

Based on the discussion in the UV-vis section, we selected PBDB-T as the donor material to fabricate bulk heterojunction (BHJ) OSCs with a conventional structure of ITO/PEDOT:PSS/PBDB-T:acceptor/PDINO/Al. The thickness of PDINO ETL was tested to be 14 nm. In order to obtain the optimized device performances, different additives such as 1.8-diiooctane (DIO), methylnaphthalene (CH_3–N) and chloronaphthalene (CN) and solvent vapor annealing (SVA) were tested and the photovoltaic data and AFM images were summarized in SI. The optimized photovoltaic parameters were summarized in Table 2. The *J-V* curves of the optimized devices were shown in Fig. 6a. After device optimizations, especially with SVA treatments, **TTIC-M**, **TTIC** and **TTIC-F** based devices gave high PCEs of 9.97%, 10.87% and 9.51%, respectively. Impressively high J_{sc} with values of 19.07, 20.50 and 21.26 mA cm^{-2} were obtained for **TTIC-M**, **TTIC** and **TTIC-F** based devices, which was contributed to the complementary and broad absorptions of donor polymer and the NFAs in the range of 300 to 900 nm. In addition, after introduction of methyl and fluorine in the end groups, the V_{oc} increased (0.83 V) and decreased (0.71 V) in comparison with that of **TTIC** (0.80 V), which was consistent with the variation tendency of the LUMO energy levels of the acceptors. Meantime, the photon energy loss (E_{loss}) was calculated using the formula $E_{loss} = E_g - eV_{oc}$. The E_{loss} values of the OSCs are 0.58–0.64 eV, which are relatively small in OSC devices. EQE spectra were used to further explain the J_{sc} values. These devices all show high photoelectron conversion efficiency ranging from 300–900 nm (Fig. 6b), suggesting the complementary absorption properties between the **PBDB-T** donor and **ITIC** derivatives.

Mobility

The hole and electron mobility were measured by the SCLC method (Fig. 7) and the mobility data were summarized in Table 3. After SVA for 90 s, **TTIC-M**, **TTIC** and **TTIC-F** all possess high hole and electron mobility $0.87 \times 10^{-4}/0.86 \times 10^{-4}$, $1.63 \times 10^{-4}/1.61 \times 10^{-4}$ and $1.29 \times 10^{-4}/1.38 \times 10^{-4}$ cm^2 V^{-1} s^{-1} with a μ_h/μ_e ratio of 1.01, 1.01 and 0.93, respectively. The relatively high and balanced charge transport properties bring the higher FF and J_{sc} values.

Film morphology

AFM was utilized to investigate the surface morphology of the blend films under tapping-mode (Fig. 8). After SVA, the blend films show suitable root-mean-square

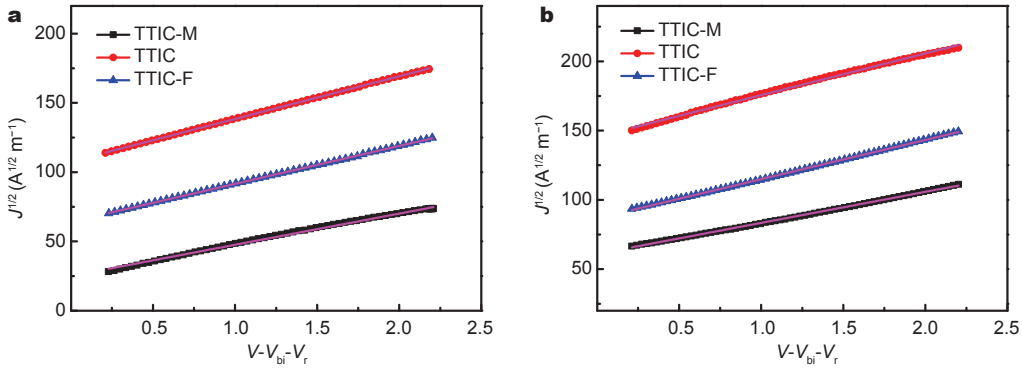

Figure 7 The hole (a) and electron (b) mobilities.

Table 3 The mobility of **TTIC-M**, **TTIC** and **TTIC-F** devices after SVA for 90 s

Compound	μ_h (10^{-4} cm^{-2} V^{-1} s^{-1})	μ_e (10^{-4} cm^{-2} V^{-1} s^{-1})	μ_h/μ_e
TTIC-M	0.87	0.86	1.01
TTIC	1.63	1.61	1.01
TTIC-F	1.29	1.38	0.93

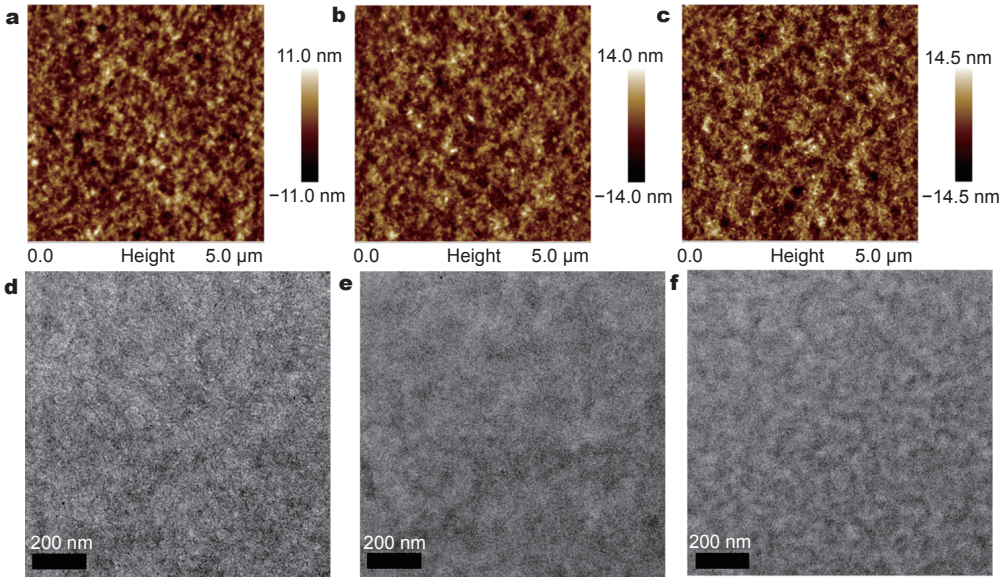

Figure 8 The AFM images of the blend films **PBDB-T/TTIC-M** (a), **TTIC** (b) and **TTIC-F** (c) with SVA for 90 s and the TEM images below (d, e, f).

(RMS) roughness of 2.78, 3.39 and 3.95 nm, respectively. As shown in the AFM and the corresponding transmission electron microscopy (TEM) images, they all show good phase separation with appropriate domain size. From the TEM images, the nanoscale wormlike domain can be observed in the film with SVA, which is beneficial for obtaining high J_{sc} and FF.

CONCLUSIONS

In summary, three NFAs with near-infrared absorptions, **TTIC-M**, **TTIC** and **TTIC-F** were synthesized and used in OSCs devices. Blending with a wide band gap donor

polymer **PBDB-T** with a complementary absorption, **TTIC-M**, **TTIC** and **TTIC-F** based devices give high PCEs of 9.97%, 10.87% and 9.51%, respectively, with the impressively high J_{sc} over 21 mA cm^{-2}. In addition, the V_{oc} of the devices could be tuned by subtly changing the molecular LUMOs through the end groups chemical engineer. It is believed that higher efficiencies could be obtained based on the above reported NFAs and their derivatives through further material design and device optimizations.

Received 26 June 2017; accepted 24 July 2017; published online 29 August 2017

1 Ganesamoorthy R, Sathiyan G, Sakthivel P. Review: fullerene based acceptors for efficient bulk heterojunction organic solar cell applications. Sol Energ Mater Sol Cells, 2017, 161: 102–148
2 Lai YY, Cheng YJ, Hsu CS. Applications of functional fullerene materials in polymer solar cells. Energ Environ Sci, 2014, 7: 1866
3 Jamieson FC, Domingo EB, McCarthy-Ward T, *et al.* Fullerenecrystallisation as a key driver of charge separation in polymer/fullerene bulk heterojunction solar cells. Chem Sci, 2012, 3: 485–492
4 Troshin PA, Hoppe H, Renz J, *et al.* Material solubility-photovoltaic performance relationship in the design of novel fullerene derivatives for bulk heterojunction solar cells. Adv Funct Mater, 2009, 19: 779–788
5 Prachumrak N, Sudyoadsuk T, Thangthong A, *et al.* Improvement of D–π–A organic dye-based dye-sensitized solar cell performance by simple triphenylamine donor substitutions on the π-linker of the dye. Mater Chem Front, 2017, 1: 1059–1072
6 Huang J, Wang H, Yan K, *et al.* Highly efficient organic solar cells consisting of double bulk heterojunction layers. Adv Mater, 2017, 29: 1606729
7 Kan B, Li M, Zhang Q, *et al.* A series of simple oligomer-like small molecules based on oligothiophenes for solution-processed solar cells with high efficiency. J Am Chem Soc, 2015, 137: 3886–3893
8 Zhang Q, Kan B, Liu F, *et al.* Small-molecule solar cells with efficiency over 9%. Nat Photon, 2014, 9: 35–41
9 Meng D, Sun D, Zhong C, *et al.* High-performance solution-processed non-fullerene organic solar cells based on selenophene-containing perylene bisimide acceptor. J Am Chem Soc, 2016, 138: 375–380
10 Lin Y, Zhao F, Wu Y, *et al.* Mapping polymer donors toward high-efficiency fullerene free organic solar cells. Adv Mater, 2017, 29: 1604155
11 Liu Y, Zhang H, Sun Y, *et al.* A-D-A-type small molecular acceptor with one hexyl-substituted thiophene as π bridge for fullerene-free organic solar cells. Sci China Mater, 2017, 60: 49–56
12 Chen W, Zhang Q. Recent progress in non-fullerene small molecule acceptors in organic solar cells (OSCs). J Mater Chem C, 2017, 5: 1275–1302
13 Chen W, Yang X, Long G, *et al.* A perylene diimide (PDI)-based small molecule with tetrahedral configuration as a non-fullerene acceptor for organic solar cells. J Mater Chem C, 2015, 3: 4698–4705
14 Zhao W, Zhang S, Hou J. Realizing 11.3% efficiency in fullerene-free polymer solar cells by device optimization. Sci China Chem, 2016, 59: 1574–1582
15 Cui Y, Yao H, Gao B, *et al.* Fine-tuned photoactive and interconnection layers for achieving over 13% efficiency in a fullerene-free tandem organic solar cell. J Am Chem Soc, 2017, 139: 7302–7309
16 Zhao W, Li S, Yao H, *et al.* Molecular optimization enables over 13% efficiency in organic solar cells. J Am Chem Soc, 2017, 139: 7148–7151
17 Chen S, Liu Y, Zhang L, *et al.* A wide-bandgap donor polymer for highly efficient non-fullerene organic solar cells with a small voltage loss. J Am Chem Soc, 2017, 139: 6298–6301
18 Zhong L, Gao L, Bin H, *et al.* High efficiency ternary nonfullerene polymer solar cells with two polymer donors and an organic semiconductor acceptor. Adv Energ Mater, 2017, 7: 1602215
19 Liu F, Zhou Z, Zhang C, *et al.* Efficient semitransparent solar cells with high NIR responsiveness enabled by a small-bandgap electron acceptor. Adv Mater, 2017, 29: 1606574
20 Yang L, Zhang S, He C, *et al.* New wide band gap donor for efficient fullerene-free all-small-molecule organic solar cells. J Am Chem Soc, 2017, 139: 1958–1966
21 Yu R, Zhang S, Yao H, *et al.* Two well-miscible acceptors work as one for efficient fullerene-free organic solar cells. Adv Mater, 2017, 29: 1700437
22 Lin Y, Zhao F, He Q, *et al.* High-performance electron acceptor with thienyl side chains for organic photovoltaics. J Am Chem Soc, 2016, 138: 4955–4961
23 Li S, Ye L, Zhao W, *et al.* Energy-level modulation of small-molecule electron acceptors to achieve over 12% efficiency in polymer solar cells. Adv Mater, 2016, 28: 9423–9429
24 Yao H, Cui Y, Yu R, *et al.* Design, synthesis, and photovoltaic characterization of a small molecular acceptor with an ultra-narrow band gap. Angew Chem Int Ed, 2017, 56: 3045–3049
25 Dai S, Zhao F, Zhang Q, *et al.* Fused nonacyclic electron acceptors for efficient polymer solar cells. J Am Chem Soc, 2017, 139: 1336–1343
26 Qiu N, Zhang H, Wan X, *et al.* A new nonfullerene electron acceptor with a ladder type backbone for high-performance organic solar cells. Adv Mater, 2017, 29: 1604964
27 Kan B, Feng H, Wan X, *et al.* Small-molecule acceptor based on the heptacyclic benzodi(cyclopentadithiophene) unit for highly efficient nonfullerene organic solar cells. J Am Chem Soc, 2017, 139: 4929–4934
28 Cheng YJ, Yang SH, Hsu CS. Synthesis of conjugated polymers for organic solar cell applications. Chem Rev, 2009, 109: 5868–5923
29 Zhang Q, Wang Y, Kan B, *et al.* A solution-processed high performance organic solar cell using a small molecule with the thieno[3,2-b]thiophene central unit. Chem Commun, 2015, 51: 15268–15271
30 Cao Q, Xiong W, Chen H, *et al.* Design, synthesis, and structural characterization of the first dithienocyclopentacarbazole-based n-type organic semiconductor and its application in non-fullerene polymer solar cells. J Mater Chem A, 2017, 5: 7451–7461
31 Liu F, Zhou Z, Zhang C, *et al.* A thieno[3,4-b]thiophene-based non-fullerene electron acceptor for high-performance bulk-heterojunction organic solar cells. J Am Chem Soc, 2016, 138: 15523–15526
32 Xiao B, Tang A, Zhang J, *et al.* Achievement of high V_{oc} of 1.02 V for P3HT-based organic solar cell using a benzotriazole-containing non-fullerene acceptor. Adv Energ Mater, 2017, 7: 1602269

33 Qian D, Ye L, Zhang M, *et al.* Design, application, and morphology study of a new photovoltaic polymer with strong aggregation in solution state. Macromolecules, 2012, 45: 9611–9617
34 Wang W, Yan C, Lau TK, *et al.* Fused hexacyclic nonfullerene acceptor with strong near-infrared absorption for semitransparent organic solar cells with 9.77% efficiency. Adv Mater, 2017, 49: 1701308
35 Bronstein H, Ashraf RS, Kim Y, *et al.* Synthesis of a novel fused thiophene-thieno[3,2-b]thiophene-thiophene donor monomer and co-polymer for use in OPV and OFETs. Macromol Rapid Commun, 2011, 32: 1664–1668

Acknowledgements The work was supported by the Minstry of Science and Technology (2014CB643502), the National Natural Science Foundation of China (91633301, 51422304 and 91433101), PCSIRT (IRT1257) and Tianjin city (17JCZDJC31100).

Author contributions Gao HH, Wan X, Chen Y and Kan B designed the project. Wan X, Li C and Chen Y directed the research. Sun Y, Wan X and Zhang H fabricated and characterized the devices, Ke X finished the DFT calculation. Gao HH wrote the paper, with support from Chen Y. All authors contributed to the general discussion.

Conflict of interest The authors declare that they have no conflict of interest.

Supplementary information Supporting data are available in the online version of the paper.

Huan-Huan Gao is a PhD candidate under the supervision of Prof. Yongsheng Chen and Wan Xiangjian at Nankai University. She received her bachelor's degree in chemistry from Nanyang Normal University in 2013 and master's degree in organic chemistry from Nankai University in 2016. Her research focuses on the design and synthesis of organic photovoltaic materials.

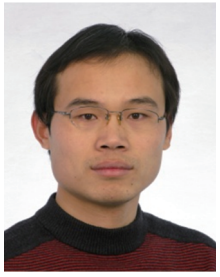

Xiangjian Wan received his PhD degree in organic chemistry from Nankai University, China, in 2006. Currently, he is a professor at Nankai University. His research interests focus on the organic functional materials design and application, especially on the solution processed small molecule OPV materials and device optimization.

Yongsheng Chen received his PhD in chemistry at the University of Victoria in 1997. From 2003, he has been a Chair Professor at Nankai University. His main research interests focus on carbon-based nanomaterials and organic functional materials for green energy applications.

窄带系非富勒烯受体用于有机太阳电池获得超过21 mA cm^{-2}的短路电流密度

高欢欢, 孙延娜, 万相见*, 阚斌, 柯鑫, 张洪涛, 李晨曦, 陈永胜*

摘要 本文设计合成了基于噻吩[3,2b]噻吩稠环受体具有不同末端基团的三个窄带系非富勒烯受体TTIC-M, TTIC和TTIC-F. 采用宽带隙聚合物PBDB-T为给体在300–900 nm光谱范围内形成了互补光吸收, 基于TTIC-M, TTIC和TTIC-F的光伏器件分别获得了高达9.97%, 10.87%和9.51%的效率和高达21 mA cm^{-2}的短路电流密度.